Multiscale model for pedestrian and infection dynamics during air travel

Sirish Namilae,[1,*] Pierrot Derjany,[1] Anuj Mubayi,[2] Mathew Scotch,[3,4] and Ashok Srinivasan[5]
[1]*Department of Aerospace Engineering, Embry-Riddle Aeronautical University, Daytona Beach, Florida 32114, USA*
[2]*SAL Mathematical, Computational and Modeling Science Center, School of Human Evolution and Social Change, Arizona State University, Tempe, Arizona 85287, USA*
[3]*Department of Biomedical Informatics, Arizona State University, Scottsdale, Arizona 85259, USA*
[4]*Biodesign Center for Environmental Security, Arizona State University, Tempe, Arizona 85257, USA*
[5]*Department of Computer Science, Florida State University, Tallahassee, Florida 32306, USA*
(Received 30 November 2016; revised manuscript received 7 March 2017; published 31 May 2017)

In this paper we develop a multiscale model combining social-force-based pedestrian movement with a population level stochastic infection transmission dynamics framework. The model is then applied to study the infection transmission within airplanes and the transmission of the Ebola virus through casual contacts. Drastic limitations on air-travel during epidemics, such as during the 2014 Ebola outbreak in West Africa, carry considerable economic and human costs. We use the computational model to evaluate the effects of passenger movement within airplanes and air-travel policies on the geospatial spread of infectious diseases. We find that boarding policy by an airline is more critical for infection propagation compared to deplaning policy. Enplaning in two sections resulted in fewer infections than the currently followed strategy with multiple zones. In addition, we found that small commercial airplanes are better than larger ones at reducing the number of new infections in a flight. Aggregated results indicate that passenger movement strategies and airplane size predicted through these network models can have significant impact on an event like the 2014 Ebola epidemic. The methodology developed here is generic and can be readily modified to incorporate the impact from the outbreak of other directly transmitted infectious diseases.

DOI: 10.1103/PhysRevE.95.052320

I. INTRODUCTION

Commercial air travel enables rapid transmission of infectious diseases across the globe. Travelers are in close proximity to each other and are susceptible to infection spread in common spaces such as airport boarding areas, lounges, security lines, and within commercial airplanes. In addition, air travel brings together people from different geographic regions with different levels of vulnerability and receptivity due to variations in immunity, ethnic background, and intervention usage across geographic areas [1]. There is direct evidence for the spread of infection within commercial airplanes for many infectious diseases including influenza [2], SARS [3], tuberculosis [4], measles [5], and norovirus [6].

Several factors affect the infection transmission in the high-occupancy enclosed environment of aircraft cabins, including cabin air quality, exposure time, flight duration, and passenger contact due to inflight movement. The high-efficiency particulate filters used in current airplanes are effective in reducing a contagion in the recirculated air [7]; however, virus shedding from infected passengers before the air can pass through filters can lead to other passengers becoming infected. In this context, passenger location and movement resulting in close contact between infective and susceptible populations is a critical component in infection spread aboard airplanes. Passengers move during boarding (ingress), deplaning (egress), and within the cabin. Susceptible passengers otherwise not exposed to the contagion may come into contact with it when they are in close proximity to infected passengers or contaminated surfaces during the high-mobility phases of passenger entry and exit. There is a strong correlation between contact rates and infection rates in a number of disease epidemics including SARS [8] and Ebola [9]. The probability of infectious disease transmission when the host and agent come into contact is inherently stochastic and depends on variations in multiple factors including infectivity (virus content in bodily fluids and rate of shedding), age, and demographic characteristics. Stochastic infection models such as the susceptible-exposed-infectious (SEI) model have been effectively used in studying such infectious disease spread [10]. In this paper we develop a hybrid model that combines a social-force-based pedestrian dynamical model with a stochastic infection transmission framework to study the effect of pedestrian dynamics on the infection spread.

Often there are limitations in modeling quantities related to real systems. Therefore, stochasticity is naturally inherent in systems, that is, there is uncertainty in its constituents. In order to address distinct types of uncertainty present in the system, we use scenario analyses into the aforementioned stochastic process based on the SEI framework to allow for variance in projections of output parameters. We quantify the uncertainty in the input parameters as well as structural uncertainty in the model itself by simulating over the design space.

As a case study, we utilize the model to assess the propagation of Ebola aboard an airplane. During the 2014–2015 Ebola epidemic, despite travel restrictions, there have been a few instances of Ebola-infected travelers using commercial airplanes in the USA and Nigeria [11–13]. Models have suggested that 7.17 infected travelers per month would have been transported through commercial airlines without air-travel restrictions [14]. Detailed pedestrian dynamics enables tracking the trajectories of passengers that is needed to assess passenger contact rates due to different air-travel policies.

*Corresponding author: namilaes@erau.edu

While all in-plane passenger movement (e.g., movement of airplane staff and passenger movement to restrooms) can contribute to infection spread, the discretionary nature of such activities requires additional uncertainty considerations and difficulty in modeling; therefore, we focus on high pedestrian density and mobility phases of airplane boarding and deplaning in this paper. Through the modeling framework developed in this paper, we assess the air-travel and passenger movement strategies that can reduce the infectious disease spread. The pedestrian movement component can be used to model different crowded locations such as airports and the stochastic infection dynamics component can be used for other directly transmitted diseases. The integrated model developed here is therefore general and can be applied to other infection studies.

II. MODEL FORMULATION

We model the motion of pedestrians using a molecular-dynamics-based social-force model [15]. Considering a pedestrian as a particle in motion, the pedestrian particle is subjected to competing forces of a person's desire to travel to a destination while impeded by obstructions (e.g., walls, chairs, and other pedestrians). The total force experienced by a pedestrian

$$\bar{F}_i = \sum \bar{f}_i = \bar{f}_i^{\text{int}} + \bar{f}_i^{\text{ped}} = m_i \bar{a}_i, \tag{1}$$

where $\bar{F}_i$ is the resulting force, $\bar{f}_i^{\text{int}}$ is the force exerted by the pedestrian in the intention to reach his or her terminus, $\bar{f}_i^{\text{ped}}$ is the resisting forces obstructing the motion, m_i is the body mass, and $\bar{v}_i$ and $\bar{a}_i$ are the instantaneous velocity and acceleration at time t, respectively.

The intention force relates the desired velocity of pedestrian i moving towards a destination $\bar{v}_{0i}$ to the actual speed v_i and is defined by

$$\bar{f}_i^{\text{int}} = \frac{m_i}{\tau}[\bar{v}_{0i}(t) - \bar{v}_i(t)]. \tag{2}$$

Here τ is a time step. We modify the equations of motion by introducing a local neighbor dependence to the desired velocity $\bar{v}_0^i(t)$. In line-forming applications like in an airplane entry or exit, the self-propelling intention force and desired velocity of the ith pedestrian is dependent on the position of the nearest pedestrian in the direction of motion, i.e., in front of the pedestrian particle in the line. To model the slowing of pedestrian particles as they approach other particles in a line, the desired velocity of the ith pedestrian $\bar{v}_0^i(t)$ in direction $\hat{e}_1$ is modified as follows:

$$\bar{v}_{0i} \cdot \hat{e}_1 = (v_A + \gamma v_B)\left(1 - \frac{\delta}{\bar{r}_i \hat{e}_1 - \bar{r}_i \hat{e}_1}\right). \tag{3}$$

Here $\hat{e}_1$ is the direction of desired motion. For example, for a passenger boarding an airplane, this could be the direction along the aisle. The term $v_A + \gamma_i v_B$ provides a distribution of desired speed for all pedestrians in the system, v_A is the deterministic component of the pedestrian speed, γ_i is a random number, and $\gamma_i v_B$ is the component of pedestrian speed that varies for each pedestrian, enabling a distribution of speeds that accounts for differences due to factors such as age and sex. In addition, $\bar{r}_i$ and $\bar{r}_k$ denote the positions of ith and kth pedestrians, where the kth pedestrian is the nearest in the $\hat{e}_1$ direction and $\bar{r}_i \hat{e}_1 - \bar{r}_k \hat{e}_1$ would be the separation between them in direction $\hat{e}_1$. Further, δ is the critical distance between two pedestrians in a line at which the rear pedestrian becomes stationary. Equation (3) ensures that the attractive force toward the destination is reduced when a pedestrian encounters another particle and the desired speed reduces to zero when the distance between them is δ.

The second part of the particle dynamics in Eq. (1) considers the repulsive-social-force term $\bar{f}_i^{\text{ped}}$ that inhibits the motion of pedestrian particles. The repulsive force is essential to ensure impenetrability of particles. For this purpose, we use the repulsive term [16] of the Lennard-Jones potential given by

$$\bar{f}_i^{\text{ped}} = \sum \bar{f}_{ij} = \sum_{i \neq j} \nabla \varphi(\bar{r}_{ij}) = \sum_{i \neq j} \nabla \left[\epsilon \left(\frac{\sigma}{r_{ij}} \right)^{12} \right], \tag{4}$$

where ϵ and σ are constants and r_{ij} is the distance between the ith and jth pedestrians. The equation of motion in (1) is numerically integrated to obtain the velocities and positions in the subsequent time steps. We apply this approach to pedestrian movement in airplanes to obtain the trajectories of pedestrian movement for different boarding and deplaning methods. Note that Eqs. (1)–(4) are in two-dimensional space in the plane of pedestrian movement.

There are several parameters in the pedestrian dynamics model, such as maximum walking speed $v_A + v_B$, random variation γ_i, distance parameter δ, two parameters for the Lennard-Jones repulsive-force terms (ϵ and σ), and aisle delay for luggage. There is experimental data available for some of the parameters such as the range of walking speed [17,18]. Also, the observed exit times and passenger flow rate for some commercial airplanes are available in the literature [19,20]. To obtain the estimates of other model parameters that represent realistic model behavior of an outbreak, we vary the parameters over a large design space. In our earlier study [21] we used a parameter sweep on 60 000 processors to determine the parameters that match the available observed data of deplaning [19,20]. We have been able to match the pedestrian dynamics model with experimental data on flow rates and exit times for five different airplane seating configurations for which test data are available. In addition, we have also been able to capture qualitative features such as front to back unloading and hallway congestion [21]. The pedestrian dynamics parameters obtained through our earlier work [21] are used in the model and are tabulated in Table I.

The pedestrian trajectory information from the above model (1)–(4) is integrated with a discrete-time stochastic SEI model for infection transmission described below [Eqs. (5) and (6)]. Note that in the context of air travel of a few hours, newly exposed (and infected) passengers do not become infectious. The schematic in Fig. 1 depicts the overall approach of this modeling study.

From a population of N passengers, if i_c^0 represents the number of infective passengers at a given time with age of infection of c, then the number of susceptible individuals at

TABLE I. Parameters and data ranges used in the computational models.

Parameters	Definition	Estimate or range	Reference or notes
$\bar{v}_{0i}$	walking speed (no obstructions)	1.07–1.55 m/s	[18,21]
γ_i	random number	0–1	[21]
δ	distance parameter (distance between people in a stationary line)	0.405 m	[21]
ϵ	repulsive-force field parameter	16	[21]
σ	repulsive-force field parameter	0.86 m	[21]
p_c	infectivity of individual as a function of age of infection (c days).	0.01–0.098	based on [23] (see Fig. 2)
D	maximum number of days for virus incubation	1–21 d	[23]
i_c^0	number of infectives with an age of infection of c days	1	only one infective per plane assumed

time t, $S(t)$, is given by

$$S(t) = N - \sum_{c=1}^{d} i_c^0 = N - I(t), \tag{5}$$

where c varies between 1 and a maximum of d days of infection and $I(t)$ is the total number of infected individuals in the modeled population. In the current model, we consider that there is one infective individual with Ebola in a given population that fills an airplane; however, this number can be higher for more common infectious diseases like influenza. We also assume that the initial number of exposed individuals in the system is zero.

When these i_c^0 infective individuals come into contact with m_i susceptible individuals estimated by the pedestrian movement model, the newly infected and the probability of their infection can be estimated using a binomial distribution. In the context of air travel, the model population is relatively small (a few hundred passengers), hence, contacts are few. We assume that probability of an individual infecting each susceptible individual is small and the number of susceptible individuals as compared to the number of infected (or exposed) individuals is larger. Under this assumption, we approximated a binomial distribution using a Poisson distribution. The newly infected individuals at time t and the probability of their infection is

$$I(t) \sim \mathcal{P}\left(\sum_{c=1}^{d}\left[p_c \sum_{i=1}^{i_c^0}\left(\frac{m_i(t-1)s_{r_i}(t-1)}{N}\right)\right]\right). \tag{6}$$

Here an infective individual with infectivity p_c placed in a susceptible population would expose $m_i p_c$ members at time t. In addition, s_{r_i} represents the number of susceptible individuals within the radius r_i of the infectious individual where infection is possible. The use of the Poisson distribution $\mathcal{P}$ accounts for demographic stochasticity and variations in susceptibility of the population.

The probability distribution of infection transmission varies depending on the incubation periods and transmission rates for specific diseases and is a primary input datum required for the stochastic infection transmission model. For example, for the Ebola virus the mean incubation period is 12.7 days [22], with a logarithmic increase in virus levels in blood during acute illness phase [23]. The RNA virus copies in the serum are indicative of the transmission probability and we used the corresponding Center for Disease Control and Prevention (CDC) data [23] to obtain the infectivity profile shown in Fig. 2. Since there is no possibility of mortality by infection in the short time scale of the model, we used the weighted (by sample size) average of both fatal and nonfatal data from [23] to compute the probabilities in Fig. 2.

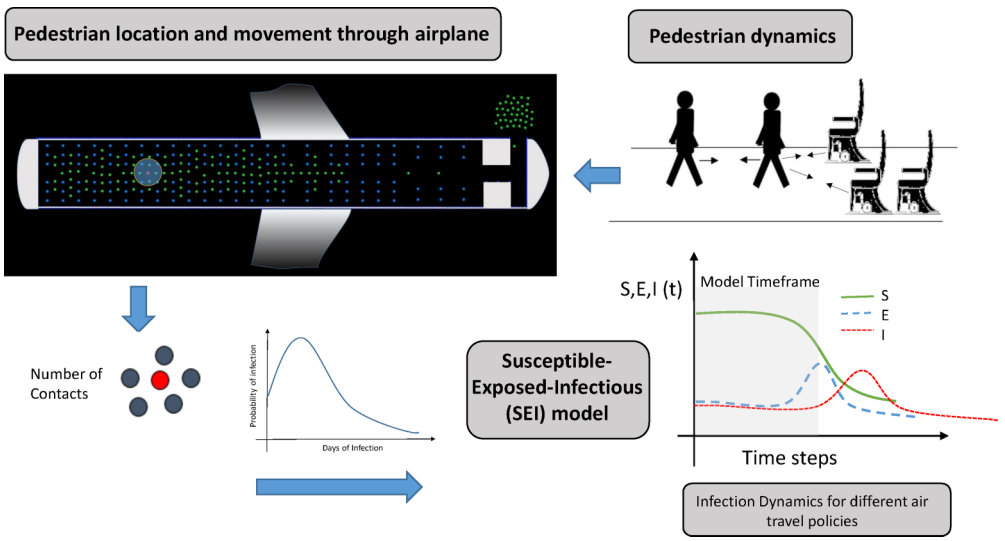

FIG. 1. Schematic depiction of the overall modeling approach.

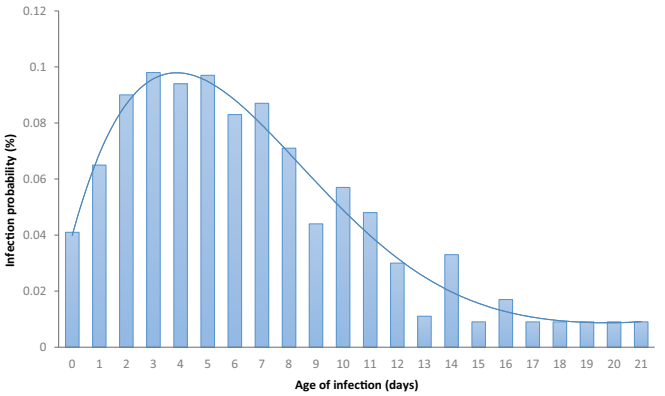

FIG. 2. Distribution of the probability of infection vs days since the onset of symptoms for the Ebola virus, modified and distribution generated using CDC data for RNA copies in serum [23].

The overall model can be adapted to other directly transmitted infectious diseases as well as other crowded locations (e.g., airport security lines) by modifying the infectivity input and the control parameters in Table I. Here we used the integrated model to study infection transmission inside an airplane. Inherent uncertainties in human behavior and stochasticity in infection spread make precise prediction of the number of infections difficult. Instead, we identify policies and passenger movement strategies that generally lead to reducing the spread of infectious diseases.

III. RESULTS AND DISCUSSION

We consider the situation with one infected individual with Ebola traveling on a commercial airplane. The infective passenger onboard is not identifiable; therefore, we varied the seating position of the infected individual through all the seats in the airplane. At each seating location of the infective individual, we obtained the mean number of newly infected members and corresponding discrete Poisson distribution using the above formulation. We combined these distributions to evaluate the probability of k newly infected passengers when an infected individual is on the airplane at any possible seating position. The mean number of newly infected individuals is the key measure we use in comparing the infection spread using different boarding and deplaning strategies. We used this approach to evaluate air-travel policies such as boarding strategies and airplane seating capacity that impact infectious disease spread.

The boarding and exiting strategies have been investigated in earlier studies with respect to minimizing the turn-around time of airplanes at boarding gates (see, e.g., [19,20]). Several passenger ingress strategies such as random, outside-in, back-to-front, columnwise, zone or section style enplanement have been studied. We compare a few of the boarding strategies with respect to the spread of infections. In Fig. 3 we show that the three-section boarding method has the highest mean and thus represents the worst strategy for reducing spread of infection. Interestingly, many current airlines use such a strategy with multiple zones or sections. In this method passengers sitting in the front of the aircraft (e.g., first class) board first followed by a middle zone and then the back section of the airplane. Because of this pattern, the passageway is filled with passengers waiting to get to their seats, resulting in clustering and increased exposure with infected passenger and therefore resulting in a higher number of newly infected passengers. The columnwise method, used here, is the same as the outside-inside strategy in a front-to-back manner. This scheme also results in more infected members. For the random and two-section boarding, passengers close together in a queue may be seated in seats that are wide apart. This leads to arbitrary movement of passengers along the cabin, preventing clustering of a group of travelers around the infected passenger, which in turn reduces infection transmission. The two-section and random boarding have the same mean value of two newly infected, although the infection transmission for the

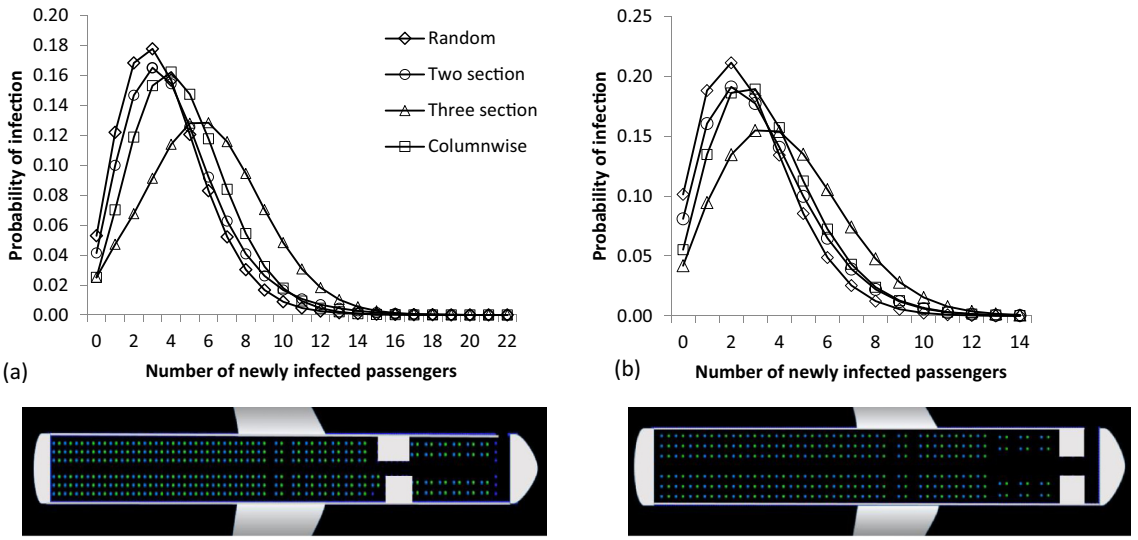

FIG. 3. Infection distribution profile for different boarding strategies for (a) a Boeing 757-200 capable of seating 182 passengers and (b) an Airbus A320 capable of seating 144 passengers. The pictures on the bottom show the corresponding aircraft seating configurations with seats (blue dots) and pedestrians (green dots).

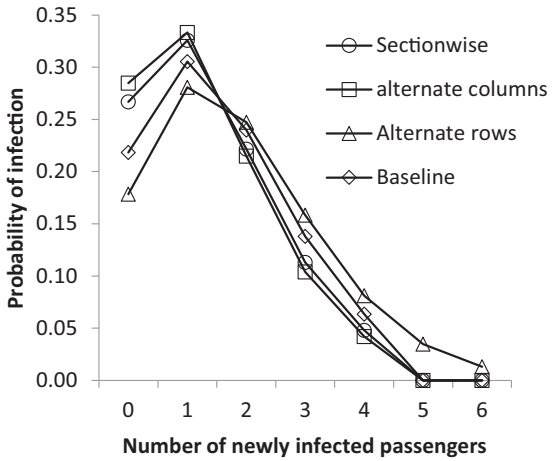

FIG. 4. Infection distribution profile for different deplaning strategies for a 182-seat Boeing 757.

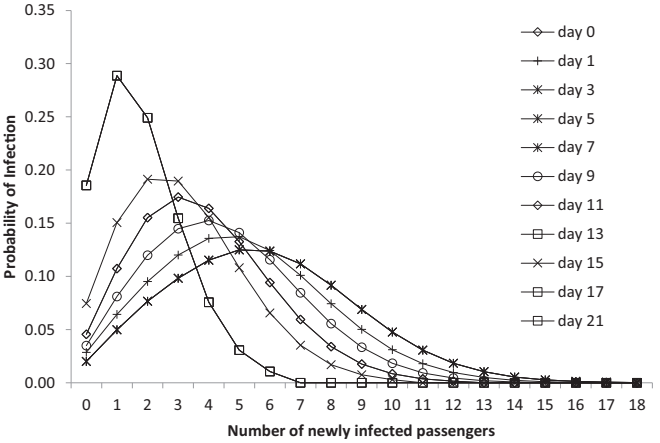

FIG. 6. Infection distribution profile varying the days of infection for the index case. A three-zone boarding strategy for a 182-passenger-seating configuration is used for these simulations.

two-section strategy results in a lower probability of infection at the mean. A two-section strategy involves dividing the plane into two sections and the passengers are randomly boarded within these sections. Our model suggests that this approach may be a good choice to reduce infection transmissions during boarding. We find a similar pattern of results for the 144-seat Airbus A320 seating configuration as well as the 182-seat Boeing 757-200 seating configuration [see Figs. 3(a) and 3(b)]. In these simulations (Figs. 3–5) the airplanes contain a single Ebola-infected passenger with infectivity, corresponding to one day of infection in an unidentified seating location with a contact radius of 1.2 m.

We followed a similar approach for the deplaning strategies. We found that deplaning had a smaller impact on infection dynamics because of the lower number of new contacts and lower time of exposure during the comparatively faster process. In Fig. 4 we show a comparison of deplaning strategies for the 182-seat Boeing 757 seating configuration. The different deplaning strategies such as alternating columns, alternating rows, zonewise, and baseline (closest to exit are out first) result in a similar number of mean infective individuals. When we compare the probabilities, alternate rows and baseline

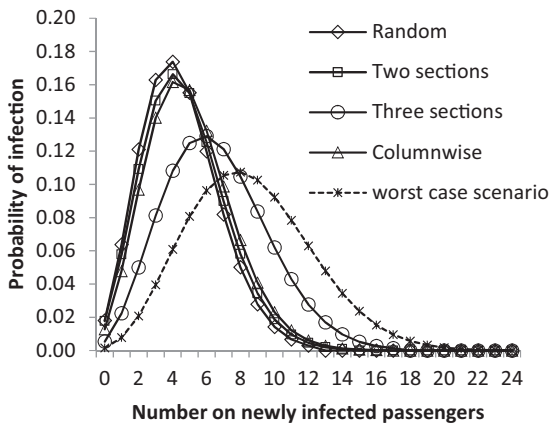

FIG. 5. Infection distribution profile for combined baseline egress with different boarding strategies for a 182-seat Boeing 757.

strategies are marginally better. In Fig. 5 we compute the mean infective individuals by combining the egress, ingress, and in-plane movement. It is apparent that other pedestrian movement strategies can be better than the boarding using multiple zones. We show the worst case situation where an infected individual with peak infectivity is seated at a location that results in the highest number of contacts.

There is an inherent uncertainty in the human movement behavior as well as the stochasticity in the infection model. Many parameters affect the simulations, including airplane size and seating arrangement, the number of infective passengers, the infectivity characterized by days post onset of symptoms, the radius of infection, which in turn depends on transmission mechanics (e.g., coughing and talking), and the susceptibility of population. It is necessary to assign values for some of these parameters for deterministic analysis, however the uncertainty in these parameters needs to be quantified to assess effective air-travel policies under a broad set of conditions. We have studied the variations in some of those parameters.

According to the CDC, data on nonfatal Ebola infection lasts for 21 days post onset of symptoms, with highest virus shedding rates and correspondingly highest infectivity in days 3–5 of disease development [23]. The three-zone-boarding simulations are repeated by varying the number of days of infection for an infective person as we show in Fig. 6. The number of mean newly infected passengers clearly varies with the infectivity of the index passenger. During a known outbreak, reported infected passengers will most likely be grounded for further monitoring, but there have been three cases of potentially newly infected passengers traveling through commercial airplanes from the 2014 epidemic [11–13]. A medical professional traveled in two commercial airplanes on October 10 and October 13, 2014 within the United States [11]. The index case was tested and confirmed to be infected on October 15; however, it is uncertain if the person was infectious and exhibiting symptoms during the travel dates. Contact tracing indicated no further infections. According to our simulations, the probability of zero new infected cases is about 7% with a fully loaded flight. Note that there was a large number of vacant seats in one of the flights,

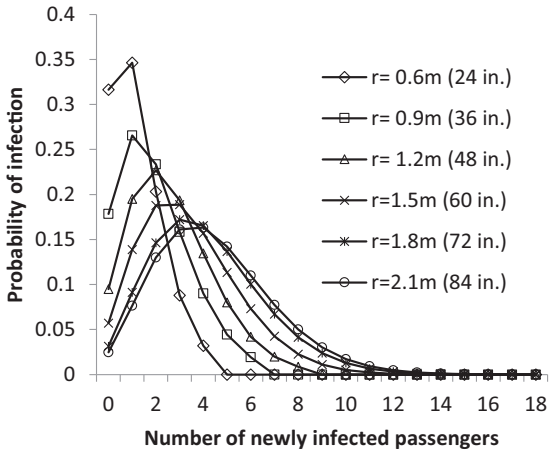

FIG. 7. Infection distribution profile varying the contact radius for infection transmission. A three-zone boarding strategy for a 182-passenger-seating configuration is used for these simulations.

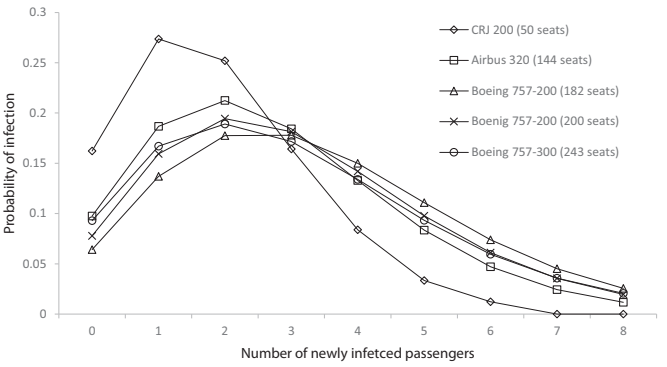

FIG. 8. Infection distribution profile for random boarding strategy, varying the airplane size.

which would have increased this probability. We cannot make a direct comparison because it is not known if the index case was infectious [11].

Another critical model parameter is the contact radius, which is the minimum distance at which a susceptible passenger in the proximity of the infective individual can be potentially infected. The distance to which particles travel depends on the particle size and associated fluid mechanics in expiratory events such as coughing and talking [24]. Experimental investigations measure particle size in these expiratory events to be in the range of 0.1–10 μm [25–27]. Droplets emanating from cough of 30 μm and smaller have been estimated to travel over 2 m [24,27]. The transmission distance also depends on specific disease, for example, SARS has been transmitted by short-range droplet-based as well as longer-range airborne mechanisms [28]. The primary mode of transmission for Ebola is through contact droplets, but studies with monkeys indicate possible transfer through aerosols [29]. Mangili and Gendreau [30] indicate large-droplet and airborne mechanisms are possibly highest risk transmission mechanisms during air travel.

We account for the effect of environmental variation and transmission methods on the contact radius by varying it from 0.6 m (24 in.) to 2.1 m (84 in.), as we show in Fig. 7. The typical seat width on airplanes is 18 in. (0.45 m). We consider a distance between passenger particles of 24 in. (0.61 m) as a touching distance. The lower end of the range in Fig. 7 signifies a contact-based and large-droplet mechanism, while a larger contact radius may be more relevant for aerosol-based mechanisms. As expected, the number of newly infected passengers is lower when the contact radius is lower.

Next we considered the size and the seating capacity of the airplane. In Fig. 8 we show the effect of airplane size with a random boarding strategy. Smaller airplanes such as CRJ-200 are better in reducing the spread of infection compared to larger capacity airplanes; however, the advantage with smaller seating capacity of airplanes quickly vanishes as the number of seats increase beyond 150. The smaller size of the susceptible population, the lower number of susceptible individuals within a given contact radius, and the reduced time of in-plane movement are some of the factors that benefit smaller airplanes.

The improvements obtained for individual flights by these policy changes can benefit substantially over the course of an epidemic. For example, consider the case of the 2014 Ebola epidemic: Bogoch *et al.* [14] estimate that without travel restrictions, 41 750 would have used air travel for international destinations in a given month from the highly affected countries of Liberia, Sierra-Leone, and Guinea. This is based on data from September to December 2013. They estimate that under these conditions, without travel restrictions, 7.17 infected travelers per month would travel outbound from these countries. Note that travel restrictions have resulted in very few cases of Ebola-infected travelers using commercial airplanes. We aggregate our model results based on the data from [14]. We assume that all the passengers traveling are divided equally between the A320 and Boeing 757 seating configurations considered in Fig. 3 and move according to strategies discussed earlier (Figs. 3–5). The mean number of infective individuals and the probability of infection is computed as described earlier and aggregated per month. Our model suggests that there is a 67% probability of generating more than 20 new air-travel-related infections per month using the default boarding strategies with these 144- and 182-seat-configuration airplanes. This can be reduced to less than 40% by using the better pedestrian movement strategies suggested in Figs. 3 and 4. In addition, exclusive use of small 50-seat airplanes further reduces the probability of generating 20 infected individuals to 13% probability.

IV. SUMMARY

A multiscale model combining social-force-based pedestrian dynamics and the metapopulation stochastic infection dynamics model has been formulated. The model is used to study the dynamics of Ebola virus infection on airplanes specifically during pedestrian movement related to boarding and disembarkation. Specific air-travel-related policies that potentially mitigate diseases spread are identified. The modeling approach developed here is generic and can be readily modified to other directly transmitted infectious diseases and dense pedestrian spaces.

ACKNOWLEDGMENTS

We thank Robert Pahle (Arizona State University) for useful discussions. The simulations in this paper were performed on National Center for Supercomputing Applications Bluewaters supercomputer. The authors gratefully acknowledge the support of NSF-ACI Award No. 1524972 (Simulation-Based Policy Analysis for Reducing Ebola Transmission Risk in Air Travel). S.N. and P.D. were partially supported by an ERAU-FIRST grant.

[1] M. Wilson, Emerg. Infect. Dis. **1**, 39 (1995).

[2] M. R. Moser, T. R. Bender, H. S. Margolis, G. R. Noble, A. P. Kendal, and D. G. Ritter, Am. J. Epidemiol. **110**, 1 (1979).

[3] S. J. Olsen, H. L. Chang, T. Y. Cheung, A. F. Tang, T. L. Fisk, S. P. Ooi, H. W. Kuo, D. D. Jiang, K. T. Chen, J. Lando, K. H. Hsu, T. J. Chen, and S. F. Dowell, New England J. Med. **349**, 2416 (2003).

[4] T. A. Kenyon, S. E. Valway, W. W. Ihle, I. M. Onorato, and K. G. Castro, New England J. Med. **335**, 675 (1996).

[5] K. Nelson, K. Marienau, C. Schembri, and S. Redd, Travel Med. Infect. Dis. **11**, 81 (2013).

[6] M. A. Widdowson, R. Glass, S. Monroe, R. S. Beard, J. W. Bateman, P. Lurie, and C. Johnson, J. Am. Med. Assoc. **293**, 1855 (2005).

[7] K. Bull, Travel Med. Infect. Dis. **6**, 142 (2008).

[8] M. Lipsitch, T. Cohen, B. Cooper, J. M. Robins, S. Ma, L. James, G. Gopalakrishna, S. K. Chew, C. C. Tan, M. H. Samore, D. Fisman, and M. Murray, Science **300**, 1966 (2003).

[9] C. M. Rivers, E. T. Lofgren, M. Marathe, S. Eubank, and B. L. Lewis, arXiv:1409.4607.

[10] M. J. Keeling and P. Rohani, *Modeling Infectious Diseases in Humans and Animals* (Princeton University Press, Princeton, 2008).

[11] J. J. Regan, R. Jungerman, S. H. Montiel, K. Newsome *et al.*, Morbidity Mortality Weekly Rep. **64**, 63 (2015).

[12] Healthcare worker who tested positive for Ebola flew on Frontier flight day before getting sick. Sky Talk (2014), available at http://blogs.star-telegram.com/sky_talk/2014/10/healthcare-worker-who-tested-positive-for-ebola-flew-on-frontier-flight-day-before-getting-sick.html

[13] F. Shuaib, R. Gunnala, E. O. Musa, F. J. Mahoney, O. Oguntimehin, P. M. Nguku, S. B. Nyanti, N. Knight, N. S. Gwarzo, O. Idigbe, A. Nasidi, and J. F. Vertefeuille, Morbidity Mortality Weekly Rep. **63**, 867 (2014).

[14] I. I. Bogoch, M. I. Creatore, M. S. Cetron, J. S. Brownstein, N. Pesik, J. Miniota, T. Tam, W. Hu, A. Nicolucci, S. Ahmed, J. W. Yoon, I. Berry, S. I. Hay, A. Anema, A. J. Tatem, D. Macfadden, M. German, and K. Khan, Lancet **385**, 29 (2015).

[15] D. Helbing and P. Molnár, Phys. Rev. E **51**, 4282 (1995).

[16] M. P. Allen and D. J. Tildesley, *Computer Simulation of Liquids* (Oxford University Press, Oxford, 1989).

[17] R. Knoblauch, M. Pietrucha, and M. Nitzburg, Transp. Res. Rec.: J. Transp. Res. Board **1538**, 27 (1996).

[18] J. Zębala, P. Ciępka, and A. Reza, Probl. Forensic Sci. **91**, 227 (2012).

[19] S. Marelli, G. Mattocks, and R. Merry, Aero Mag. **1** (1998).

[20] A. Wald, M. Harmon, and D. Klabjan, J. Air Transp. Manag. **36**, 101 (2014).

[21] S. Namilae, A. Srinivasan, A. Mubayi, M. Scotch, and R. Pahle, Physica A **465**, 248 (2017).

[22] M. Eichner, S. F. Dowell, and N. Firese, Osong Public Health Res. Perspectives **2**, 3 (2011).

[23] Centers for Disease Control and Prevention, *Review of Human-to-Human Transmission of Ebola Virus* (CDC, Atlanta, 2014).

[24] L. Bourouiba, E. Dehandschoewercker, and J. W. M. Bush, J. Fluid Mech. **745**, 537 (2014).

[25] L. Morawska, G. Johnson, Z. Ristovski, M. Hargreaves, K. Mengersen, S. Corbett, C. Chao, Y. Li, and D. Katoshevski, J. Aerosol Sci. **40**, 256 (2009).

[26] R. S. Papineni and F. S. Rosenthal, J. Aerosol Med. **10**, 105 (1997).

[27] J. K. Gupta, C. H. Lin, and Q. Chen, Indoor Air **19**, 517 (2009).

[28] R. P. Clark and M. L. de Calcina-Goff, J. R. Soc. Interface **6**, S767 (2009).

[29] N. Jaax, P. Jahrling, T. Geisbert, J. Geisbert, K. Steele, K. Mckee, D. Nagley, E. Johnson, G. Jaax, and C. Peters, Lancet **346**, 1669 (1995).

[30] A. Mangili and M. A. Gendreau, Lancet **365**, 989 (2005).